Inorganic Chemistry

Article

pubs.acs.org/IC

Crystallographic and Spectroscopic Insights into Heme Degradation by *Mycobacterium tuberculosis* MhuD

Amanda B. Graves,[†] Robert P. Morse,[‡] Alex Chao,[‡] Angelina Iniguez,[‡] Celia W. Goulding,[‡,§] and Matthew D. Liptak*,[†]

[†]Department of Chemistry, University of Vermont, Burlington, Vermont 05405, United States

[‡]Department of Molecular Biology & Biochemistry and [§]Department of Pharmaceutical Sciences, University of California−Irvine, Irvine, California 96297, United States

Supporting Information

ABSTRACT: Mycobacterium heme utilization degrader (MhuD) is a heme-degrading protein from *Mycobacterium tuberculosis* responsible for extracting the essential nutrient iron from host-derived heme. MhuD has been previously shown to produce unique organic products compared to those of canonical heme oxygenases (HOs) as well as those of the IsdG/I heme-degrading enzymes from *Staphylococcus aureus*. Here, we report the X-ray crystal structure of cyanide-inhibited MhuD (MhuD−heme−CN) as well as detailed ^{1}H nuclear magnetic resonance (NMR), UV/vis absorption, and magnetic circular dichroism (MCD) spectroscopic characterization of this species. There is no evidence for an ordered network of water molecules on the distal side of the heme substrate in the X-ray crystal structure, as was previously reported for canonical HOs. The degree of heme ruffling in the crystal structure of MhuD is greater than that observed for HO and less than that observed for IsdI. As a consequence, the Fe $3d_{xz}$-, $3d_{yz}$-, and $3d_{xy}$-based MOs are very close in energy, and the room-temperature ^{1}H NMR spectrum of MhuD−heme−CN is consistent with population of both a ^2E_g electronic state with a $(d_{xy})^2(d_{xz},d_{yz})^3$ electron configuration, similar to the ground state of canonical HOs, and a $^2B_{2g}$ state with a $(d_{xz},d_{yz})^4(d_{xy})^1$ electron configuration, similar to the ground state of cyanide-inhibited IsdI. Variable temperature, variable field MCD saturation magnetization data establishes that MhuD−heme−CN has a $^2B_{2g}$ electronic ground state with a low-lying ^2E_g excited state. Our crystallographic and spectroscopic data suggest that there are both structural and electronic contributions to the α-meso regioselectivity of MhuD-catalyzed heme cleavage. The structural distortion of the heme substrate observed in the X-ray crystal structure of MhuD−heme−CN is likely to favor cleavage at the α- and γ-meso carbons, whereas the spin density distribution may favor selective oxygenation of the α-meso carbon.

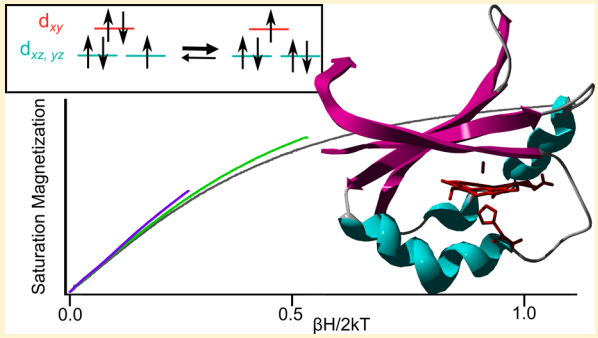

INTRODUCTION

Mycobacterium tuberculosis, the causative agent of the human disease tuberculosis, acquires the vital nutrient iron from its host. Recently, it has been shown that *M. tuberculosis* can uptake host-derived heme as an iron source.[1,2] To date, four members of this pathway have been identified and characterized: Rv0203,[3] a secreted protein that binds extracellular heme; MmpL3 and MmpL11,[4] two membrane proteins that receive heme from Rv0203; and the mycobacterium heme utilization degrader (MhuD), which catalyzes the final step of *M. tuberculosis* heme acquisition and degradation.[5,6] Recent studies strongly suggest that *M. tuberculosis* can use exogenous heme as an iron source in the absence of non-heme iron.[1,2,7] In vitro, growth of an iron siderophore-deficient strain of *M. tuberculosis* can be recovered in the presence of heme or human hemoglobin.[1] An iron siderophore-deficient strain of a similar species, *Mycobacterium bovis*, was able to survive in mice, suggesting that heme acquisition is also utilized by mycobacteria in vivo.[7] These discoveries have led researchers to suggest that proteins from the *M. tuberculosis* heme acquisition and degradation pathway, including MhuD, represent promising new anti-mycobacterial targets.[8]

Although MhuD degrades heme to non-heme iron and organic byproducts, the enzyme has features that distinguish it from canonical heme oxygenases (HOs).[5,6] The truncated, soluble forms of human and rat HO adopt α-helical folds.[9−11] HO enzymes from several pathogenic bacteria also possess α-helical folds, including *Neisseria meningitides* HemO,[12] *Corynebacterium diphtheria* HmuO,[13] and *Pseudomonas aeruginosa* PigA.[14] In contrast, the catalytically inactive, diheme-bound form of MhuD (MhuD−diheme) has a ferrodoxin-like fold similar to that of the IsdG and IsdI heme-degrading enzymes from *Staphylococcus aureus*.[5,15] In addition, the organic byproducts of MhuD-catalyzed heme degradation are unique (Figure 1). Most canonical HOs convert the porphyrin ring to α-biliverdin and carbon monoxide (CO).[16] *P. aeruginosa* PigA is an exception, where rotation of the heme substrate within the

Received: January 9, 2014
Published: June 5, 2014

   dx.doi.org/10.1021/ic500033b | *Inorg. Chem.* 2014, 53, 5931−5940

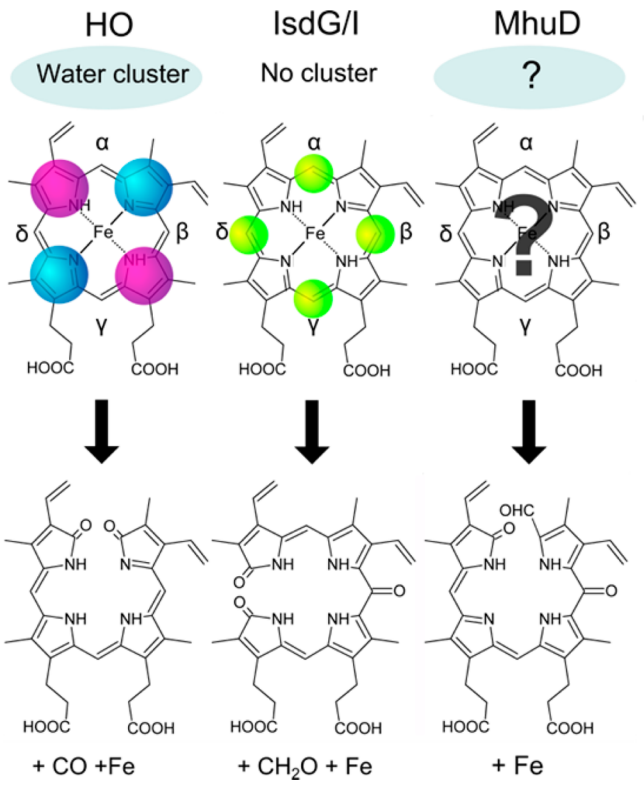

Figure 1. HO has an ordered network of active site water molecules on the distal side of the heme substrate and is believed to stabilize a ^2E_g electronic state, where spin density is delocalized onto the porphyrin pyrrole rings (violet and blue circles represent the two components of this degenerate state), producing biliverdin, CO, and iron as products. *S. aureus* IsdI has been proposed to stabilize a $^2B_{2g}$ state, with spin density delocalized onto the *α*-, *β*-, *γ*-, and *δ*-meso carbons (green circles), without a defined network of water molecules en route to staphylobilin and formaldehyde formation. *M. tuberculosis* MhuD degrades heme to mycobilin and iron, but prior to this work, the active site and electronic structures were unknown.

enzyme active site results in formation of *β*- and *δ*-biliverdin.[17,18] On the other hand, *S. aureus* IsdG and IsdI convert the porphyrin ring to a mixture of the *β*- and *δ*-isomers of staphylobilin along with a molecule of formaldehyde.[19,20] *M. tuberculosis* MhuD generates a product distinct from those of canonical HOs or IsdG/I, mycobilin, where the porphyrin ring of heme is cleaved at the *α*-meso carbon, and this carbon is retained as an aldehyde group.[6] Because MhuD generates different enzymatic products as compared to those of HOs, IsdG, or IsdI, the reaction must proceed via a unique mechanism.

On the basis of Raman, electron paramagnetic resonance (EPR), UV/vis absorption (Abs), and nuclear magnetic resonance (NMR) spectroscopy results, researchers have proposed that MhuD-catalyzed heme degradation proceeds through hydroperoxyheme and *α*-meso hydroxyheme intermediates, bypassing verdoheme, en route to mycobilin formation.[6] The first steps of this proposed mechanism (binding of molecular oxygen, reduction to hydroperoxy, and hydroxylation of the *α*-meso carbon) are identical to the generally accepted mechanism of canonical HO-catalyzed heme degradation.[16] There has been considerable debate as to whether the canonical HO reaction proceeds through a ^2E_g state with a $(d_{xy})^2(d_{xz},d_{yz})^3$ electron configuration or a $^2B_{2g}$ state with a $(d_{xz},d_{yz})^4(d_{xy})^1$ electron configuration (Figure 1).[16,21−23] However, recent EPR and Mössbauer spectroscopic data[22] and density functional theory-based hybrid quantum mechanical/molecular mechanical calculations[23] have led researchers to conclude that the enzyme active site stabilizes a ^2E_g Fe(III)−hydroperoxy state.[24] Because of its reactivity, the ^2E_g Fe(III)−hydroperoxy state has been isolated only by cryoreduction, but a similar ^2E_g state is present in cyanide-inhibited canonical HOs (HO−heme−CN).[18,25,26] An ordered network of active site water molecules on the distal side of the heme substrate, first characterized in solution by NMR spectroscopy,[27−29] favors stepwise homolytic cleavage of the hydroperoxy O−O bond followed by barrier-free attack of the *α*-meso carbon by the resulting hydroxyl radical.[21]

There remain at least two mechanistic questions regarding the MhuD-catalyzed transformation of heme to *α*-meso hydroxyheme. First, in canonical HOs, oxygen activation is expected to result in the formation of a ^2E_g state.[22,23] However, researchers have proposed that in the heme degradation reaction catalyzed by *S. aureus* IsdI, dioxygen activation results in the formation of a $^2B_{2g}$ state based on NMR characterization of cyanide-inhibited IsdI (IsdI−heme−CN).[30] These ^2E_g and $^2B_{2g}$ states have different electron and spin density distributions and, thus, different reactivities (Figure 1). Prior to this work, it was unknown whether MhuD dioxygen activation results in the formation of a ^2E_g ground state, similar to HO−heme−CN, or a $^2B_{2g}$ ground state, similar to IsdI−heme−CN. Second, there is no evidence for an ordered network of active site water molecules on the distal side of heme in the available X-ray crystal structures of heme-bound IsdG or IsdI.[30−32] These data have led to the proposal that *S. aureus* IsdI compensates for the missing network of water molecules by stabilizing a $^2B_{2g}$ state. Before this study, it was unknown whether the MhuD active site contains an ordered network of water molecules, as is the case for canonical HOs,[27−29] or if the network is absent, as is the case for *S. aureus* IsdG and IsdI.

Here, we investigate the initial steps of *M. tuberculosis* MhuD-catalyzed heme degradation using a combined crystallographic and spectroscopic approach to clarify the geometric and electronic structure of cyanide-inhibited MhuD (MhuD−heme−CN). Although MhuD−heme−CN is not an intermediate of MhuD-catalyzed heme degradation, this species is an inactive analogue for the substrate-bound form of the enzyme. Uninhibited MhuD has a high-spin monoheme form, and only the inactive, diheme form has proven to be amenable to crystallization.[5] By analogy to what is known regarding the canonical HO mechanism, MhuD-catalyzed heme degradation is expected to proceed through a low-spin $S = {}^1/_2$ state.[16] We have stabilized an $S = {}^1/_2$ monoheme form of MhuD using cyanide, and here we report the first X-ray crystal structure of a monoheme form of *M. tuberculosis* MhuD. This structure reveals that the MhuD active site has a His-ligated heme substrate lacking an organized network of water molecules on the distal side of heme. ^{1}H NMR and variable temperature, variable field (VTVH) MCD spectroscopic experiments establish the unexpected finding that at least two $S = {}^1/_2$ Fe(III) states are significantly populated at physiologically relevant temperatures. We discuss these data in terms of their implications for the initial steps of MhuD-catalyzed heme degradation.

EXPERIMENTAL SECTION

Protein Expression and Purification. All materials were purchased from Fisher Scientific unless otherwise noted. The

dx.doi.org/10.1021/ic500033b | Inorg. Chem. 2014, 53, 5931−5940

preparation of a pET-22b (Amp^r) plasmid encoding wild-type (WT) *M. tuberculosis* MhuD along with a C-terminal His_6 tag has been previously described.[5] DNA sequencing at the Vermont Cancer Center DNA Analysis Facility confirmed the sequence of the WT MhuD gene in all cell lines used for recombinant protein expression at the University of Vermont. For recombinant protein expression, the pET-22b plasmid encoding MhuD was transformed into BL21-GOLD (DE3) cells (Stratagene) as previously described.[5]

For the crystallographic studies herein, expression and purification of apo-MhuD was carried out as previously described.[5] Some minor changes were made to the apo-MhuD purification procedure for spectroscopic characterization, as noted below. Cells were lysed in 50 mM Tris, pH 7.8, 350 mM NaCl. After filtration, the lysate was loaded onto a HisPur Ni-NTA column (Pierce) equilibrated with 20 mM Tris, pH 7.8, 50 mM NaCl; washed with 20 mM Tris, pH 7.8, 50 mM NaCl, 25 mM imidazole; and washed again with 20 mM Tris, pH 7.8, 50 mM NaCl, 75 mM imidazole. Apo-MhuD was eluted using 20 mM Tris, pH 7.8, 50 mM NaCl, 400 mM imidazole. Following overnight dialysis against 20 mM Tris, pH 7.8, 50 mM NaCl, at least 8 mg/L of apo-MhuD were obtained at >99% purity. The protein concentration was determined using a Bradford assay, with bovine serum albumin (Pierce) as the standard, and purity was assessed by SDS-PAGE (Figure S1).

Preparation of heme-bound MhuD (MhuD−heme) was similar to a previously described procedure.[5] Briefly, a 0.5 mM hemin solution was prepared by initially dissolving 3.3 mg of hemin chloride in 300 μL of 1 M NaOH, to which 20 mM Tris, pH 7.4, 50 mM NaCl were added to a final volume of 10 mL. The pH of the hemin solution was adjusted to 7.4 using HCl. The final concentration of the prepared heme was determined using ε_{385} = 58.44 mM^{-1} cm^{-1}.[33] The MhuD−heme millimolar extinction coefficient for the Soret band was determined to be 91.5 mM^{-1} cm^{-1} using the pyridine hemochrome assay.[34] The MhuD−heme−CN millimolar extinction coefficient was determined to be 121 mM^{-1} cm^{-1} for the Soret band by adding one crystal of potassium cyanide (KCN) and monitoring the Abs spectrum.

Prior to characterization, MhuD activity was tested using a previously described heme/ascorbate assay (Figure S2).[5] Free hemin is stable under similar conditions in the absence of MhuD (Figure S3). The addition of cyanide abolishes MhuD-catalyzed heme degradation. MhuD−heme−CN did not turn over upon the addition of ascorbate (Figure S4).

X-ray Crystallography. Purified apo-MhuD was exchanged into 50 mM sodium phosphate (NaPi), pH 7.4, 150 mM NaCl by concentrating and resuspending three times (Amicon). A 0.5 mM hemin solution was prepared as described above except 20 mM Tris, pH 7.4, 50 mM NaCl was replaced by 50 mM NaPi, pH 7.4, 150 mM NaCl. Several crystals of potassium cyanide (KCN) were added to the hemin solution. Purified apo-MhuD (concentrated to 100 μM) and cyanide-bound heme were combined in a 1:1.05 ratio (apo-MhuD/cyanide-bound heme). MhuD−heme−CN was concentrated to 1 mL (Amicon) and was exchanged into 50 mM NaPi, pH 7.4, 150 mM NaCl using a PD-10 desalting column (GE Healthcare). MhuD−heme−CN was concentrated to 10 mg/mL in 50 mM NaPi, pH 7.4, 150 mM NaCl for crystallization trials. MhuD−heme−CN crystallized in 1.9 M ammonium sulfate, 0.1 M sodium acetate, pH 6.0, 0.2 M NaCl. Crystals were mounted, and data was collected under cryoconditions with the addition of 40% (v/v) glycerol as cryoprotectant to the reservoir condition. The native diffraction data set was collected at a wavelength of 1.0 Å at 70 K. A MhuD−heme−CN crystal diffracted to 1.9 Å, with unit cell dimensions 40.97 × 60.40 × 78.46 Å^3 and with one dimer per asymmetric unit in space group $P2_12_12_1$. Images were indexed, integrated, and reduced using iMOSFLM.[35] The initial phases were determined by molecular replacement by autoMR in PHENIX using the MhuD−diheme structure without the heme molecules present as a search model (PDB ID 3HX9). The initial model building was performed by Autobuild in PHENIX.[36] The final model was built through iterative manual building in Coot and refined with phenix.refine.[37] During refinement, minimal restraints were placed on the heme molecule to allow for greater torsional rotation of bonds within the porphyrin ring. Minimal distance and no angle restraints were used for the iron−cyanide bond. Chains A and B of the MhuD dimeric model contain residues 2−102 and 2−101, respectively. The final dimeric model contains two heme substrates, two cyanide ligands, two acetate molecules, and 94 waters (PDB ID 4NL5). Programs from Phenix,[36] Coot,[37] and PyMOL[38] were used to analyze the stereochemistry and geometry of the models and were found to be acceptable. Data and refinement statistics are presented in Table 1. All molecular graphics were prepared with PyMOL.[38]

Table 1. X-ray Data Collection and Refinement Statistics for the Structural Determination of MhuD−heme−CN

	MhuD−heme−CN
space group	$P2_12_12_1$
unit cell dimensions (Å)	40.97 × 60.40 × 78.46
pH of crystallization condition	6.0
protein concentration (mg/mL)	10
Data Set	
wavelength (Å)	1.0
resolution range	39.23−1.90
unique reflections (total)	15989 (103418)
completeness (%)[a]	99.6 (99.9)
redundancy[a]	6.5 (6.7)
R_{merge}[a,b]	6.4 (35.5)
I/σ[a]	17.3 (4.9)
NCS copies	2
Model Refinement	
resolution range (Å)	39.23−1.90
no. of reflections (working/free)	15 935 (1595)
no. of protein atoms	1505
no. of water molecules	94
no. of heme dimer	2
no. of cyanide dimer	2
missing residues	103−105
R_{work}/R_{free} (%)[c]	17.3/22.4
Average B-Factor (Å^2)	
protein	31.9
heme and cn	27.0
water	37.6
rms Deviations	
bond lengths (Å)	0.010
bond angles (degrees)	1.098
Ramachandran Plot	
most favorable region (%)	95.43
additional allowed region (%)	4.06
disallowed region	0.51
PDB ID Code	4NL5

[a]Statistics for the highest-resolution shell are given in brackets. [b]$R_{merge} = \Sigma|I - \langle I\rangle|/\Sigma I$ [c]$R_{work} = \Sigma||F_{obs}| - |F_{calc}||/\Sigma |F_{obs}|$. R_{free} was computed identically to that of R_{work} except for where all reflections belong to a test set of 10% randomly selected data.

NMR Spectroscopy. A 0.5 mM solution of cyanide-bound heme in 20 mM Tris, pH 7.4, 50 mM NaCl was prepared as described above. Purified apo-MhuD and cyanide-bound heme were combined in a 0.9:1 ratio (cyanide-bound heme/apo-MhuD) to produce MhuD−heme−CN. Residual cyanide-bound heme and apoprotein were removed upon buffer exchange into 20 mM NaPi, pH 7.4, on a PD-10 column. A 1.5 mM sample of MhuD−heme−CN in 100% D_2O (Cambridge Isotope Laboratories) was prepared by reducing the sample volume to 600 μL in Amicon stirred cells (Millipore) followed by lyophilization for at least 12 h on a VirTis lyophilizer. The resulting powder was dissolved in 600 μL of D_2O.

dx.doi.org/10.1021/ic500033b | Inorg. Chem. 2014, 53, 5931−5940

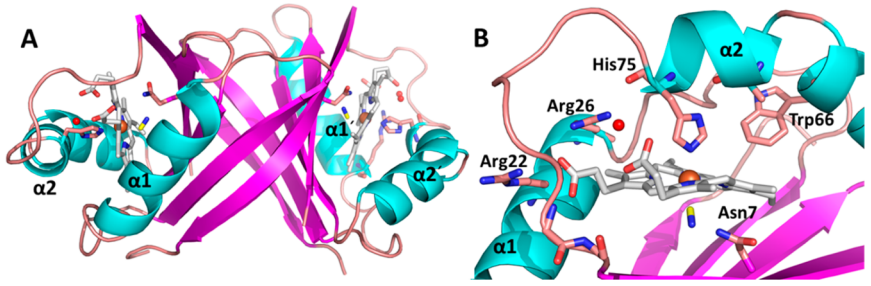

Figure 2. X-ray crystal structure of MhuD−heme−CN (PDB ID 4NL5). (A) Ribbon representation of the dimeric MhuD−heme−CN complex. (B) Ribbon representation of the MhuD−heme−CN heme-binding pocket. α-Helices and β-strands are depicted in cyan and magenta, respectively. Loops and side chain carbons are shown in salmon. All α-helices are labeled, with the second polypeptide chain differentiated by a prime symbol (′). Heme−CN, one per active site, is represented as a stick model, where nitrogen, oxygen, heme carbon, and cyano carbon atoms are in blue, red, white, and yellow, respectively. Iron atoms and ordered water molecules are depicted as orange and red spheres, respectively.

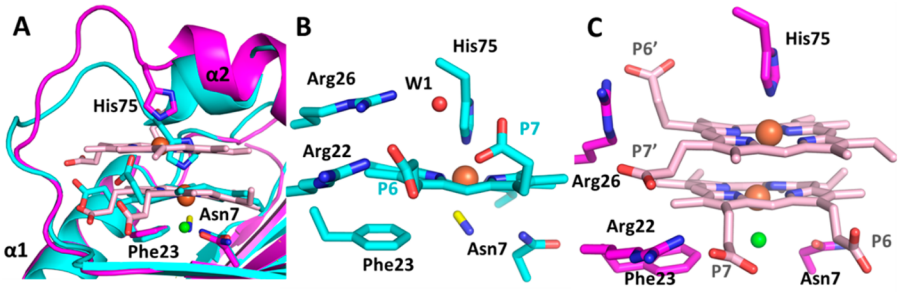

Figure 3. Structural comparison of the active sites of MhuD−heme−CN and MhuD−diheme. (A) Superposition of MhuD−heme−CN (PDB ID 4NL5, cyan) with MhuD−diheme (PDB ID 3HX9, pink) shows that α2 in MhuD−heme−CN is kinked, whereas it is extended in the MhuD−diheme structure. This kink results in MhuD−heme−CN His75 moving 4.5 Å to coordinate heme iron (orange spheres). (B, C) The orientations of most residues within the MhuD−heme−CN (B) and MhuD−diheme (C) active sites are unchanged, but Arg26 in the MhuD−heme−CN structure flips into the reduced volume active site. Heme propionates 6 and 7 are denoted by P6 and P7, respectively, and the solvent-exposed heme propionates (MhuD−diheme) are differentiated with a prime symbol (′). Heme molecules are in stick representation, with carbon atoms depicted in light cyan and light pink for MhuD−heme−CN and MhuD−diheme, respectively, and nitrogen, oxygen, and cyano carbon atoms in blue, red, and yellow, respectively. Iron atoms, an ordered Cl^- atom (MhuD−diheme structure), and water molecule (W1, MhuD−heme−CN structure) are depicted as orange, green, and red spheres, respectively.

NMR experiments were conducted at 11, 25, 35, and 42 °C on a Varian Unity Inova 500 MHz NMR spectrometer equipped with an inverse triple-resonance probe. ^{1}H NMR experiments utilized a 1.5 s relaxation delay and a 1 s acquisition time. ^{1}H Super water elimination Fourier transform (Super-WEFT)[39,40] experiments used a 50 ms τ-delay and a 50 ms acquisition time. All ^{1}H NMR and ^{1}H Super-WEFT data were referenced to sodium 2,2-dimethyl-2-silapentane-5-sulfonate (Cambridge Isotope Laboratories) via the residual water peak and processed using the ACD/Laboratories NMR Processor with 10 Hz exponential line broadening and zero filling to 65 536 points.

Optical Spectroscopy. Room-temperature Abs spectra were obtained in 20 mM Tris, pH 7.4, 50 mM NaCl between 900 and 300 nm using a Cary 100 Bio spectrophotometer with a scan rate of 600 nm/min and a 1.0 nm data interval. 280 K MCD spectra were collected in 40 mM potassium phosphate (KPi), pH 7.4, 40 mM NaCl, 60% (v/v) glycerol, and cryogenic-temperature Abs and MCD spectra were obtained in 50 mM KPi pH 7.4, 50 mM NaCl, 60% (v/v) glycerol. 280 K MCD, cryogenic temperature Abs and cryogenic-temperature MCD spectra were acquired using a home-built setup consisting of a Jasco J-815 spectropolarimeter and an Oxford SM4000-8T Spectromag controlled by a Mercury iTC temperature controller and a Mercury iPS power supply. Spectral data was acquired with a 1.0 nm bandwidth, 0.25 s integration time, 0.5 nm data pitch, and 200 nm/min scanning speed. VTVH MCD saturation magnetization curves were measured at 2, 5, and 10 K for the Soret band trough at 424 nm. Simulated VTVH MCD saturation magnetization curves were generated using the VTVH 2.1.1 program.[41,42] The simulations of models 2 [bis(1-methylimidazole)ferric tetramesitylporphyrinate] and 3 [bis(4-cyanopyridine)ferric tetramesitylporphyrinate] represent *xy*-polarized transitions of an $S = {}^1/_2$ center with **g** tensors of [1.52, 2.33, 2.90] and [2.57, 2.57, 1.42], respectively.[43]

RESULTS

X-ray Crystallography. The crystal structure of MhuD−diheme was previously determined, which revealed two stacked heme molecules in the MhuD active site. However, no heme-degradation activity was observed by MhuD−diheme, and only the monoheme complex is capable of degrading heme.[5] To observe MhuD in its monoheme active conformation, we determined the structure of MhuD−heme−CN to 1.9 Å resolution, with one homodimer in the asymmetric unit. MhuD−heme−CN retains its ferrodoxin-like $\alpha + \beta$-barrel fold, as observed for MhuD−diheme;[5] however, only one bound molecule of heme is observed in each active site (Figure 2A). In accord with previously reported spectroscopic data,[6] His75 coordinates the iron of MhuD−heme−CN on its proximal side (2.1 Å, Figure 2B), and the His75 imidazole ring is hydrogen (H)-bonded to the backbone carbonyl of Ala71. A fully occupied cyano group was modeled into the electron density observed on the distal side of the heme iron, with an Fe−C bond length of 2.1 Å. The bound CN atoms refine with B-factors of approximately 22 Å^2, similar to those of the heme irons, and fit the electron density well (Figure S5). The CN ligands are observed in a bent coordinating mode, with Fe−C−N angles of 118 and 120° for chains A and B, respectively, whereas the Fe−C−N bonds are nearly perpendicular to the

dx.doi.org/10.1021/ic500033b | Inorg. Chem. 2014, 53, 5931−5940

porphyrin plane in the IsdI−heme−CN structure, with Fe−C−N angles of 171° and 158°.[30] The Fe−C−N angle observed for MhuD−heme−CN is more similar to the 139° angle seen in cyanide-inhibited rat heme oxygenase (rHO−heme−CN; PDB ID 2E7E) at pH 6.8.[44] In the MhuD−heme−CN active site, the CN ligand forms an H-bond with Asn7 NH1 and points toward pyrrole ring A, which separates the γ- and δ-meso carbons. Furthermore, the CN-inhibited heme substrate is stabilized by hydrophobic interactions with Ile9, Phe23, Phe39, Val53, Thr55, Phe63, and Trp66; H-bonds between propionate 6 and Arg22 NH1, Arg26 NH2, and the Val83 backbone amide; and H-bonds between the bent propionate 7 and a water molecule (W1), which in turn H-bonds to Arg26 NH1.

The MhuD−diheme and MhuD−heme−CN structures superimpose with a root-mean-square deviation (rmsd) of 0.29 Å over all Cα atoms.[5] Within the active site pocket, the heme substrate overlays with the solvent-protected heme from the MhuD−diheme structure; however, the modeled heme is rotated 180° about the $\alpha-\gamma$ axis (Figure 3A). Additionally, there is an increase in heme out-of-plane distortion. The distortions of the hemes in MhuD−heme−CN (1.4 and 1.5 Å) are more severe than those in the solvent-protected heme from MhuD−diheme (0.7 Å), as analyzed by normal-coordinate structural decomposition.[45] It was suggested that Phe22 contributes to heme ruffling, the b_{1u} component of the heme out-of-plane distortion, in IsdG by contacting the γ-meso carbon.[19,31] In the MhuD−diheme and MhuD−heme−CN structures, the side chains of the corresponding residue, Phe23, overlay, suggesting that Phe23 does not contribute to ruffling, as the MhuD−diheme solvent-protected heme is planar compared to the distorted MhuD−heme−CN porphyrin ring (Figure 3A). However, the MhuD−diheme second solvent-exposed heme may play a role in the planar nature of the solvent-protected heme. The most notable structural differences are within the α2 helix and the subsequent loop region surrounding the active site (Figure 3A). In MhuD−heme−CN, the α2 helix is kinked after residue Asn68, whereas in the MhuD−diheme structure, this helix (α2) is extended. This kink results in the movement of His75 (4.5 Å) so that it may coordinate with heme iron in the MhuD−heme−CN structure (Figure 3B). Furthermore, there is one notable altered side chain conformation, Arg26, between the MhuD−heme−CN and MhuD−diheme structures. In the MhuD−diheme structure, Arg26 forms an H-bond with both propionate 6 (P6′) and propionate 7 (P7′) from the solvent-exposed heme but not with the solvent-protected heme molecule (Figure 3C). However, in MhuD−heme−CN, Arg26 is flipped into the reduced volume heme active site, where it H-bonds to an active site water molecule (W1), which in turn H-bonds to the carbonyl oxygen of His75 and heme propionate 7 (P7), whose orientation is rotated toward the active site water (W1, Figure 3B). Arg26 is also in H-bonding distance to heme propionate 6 (P6). One could speculate that the ordered water and alternative conformation of the Arg26 side chain may stabilize the otherwise flexible loop to form a stable monoheme active site. The position of this water molecule is conserved in both active sites of the MhuD dimer; however, in one of two active sites of the dimer, there is a second water molecule that also H-bonds with Arg26 (not shown).

NMR Spectroscopy. Previously, ^{1}H NMR spectroscopy revealed that the electronic ground state of HO−heme−CN is ^2E_g,[18,25,26] whereas the ground state of IsdI−heme−CN is $^2B_{2g}$.[30] To help identify the electronic ground state of MhuD−heme−CN, we have acquired the ^{1}H NMR spectrum at 25 °C (Figure 4). Because several of the hyperfine-shifted resonances in the ^{1}H NMR spectrum of MhuD−heme−CN have low intensity, we acquired a ^{1}H Super-WEFT spectrum to better detect signals from the fast-relaxing resonances. On the downfield side of the "diamagnetic" (0−10 ppm) envelope, two relatively broad peaks are detected at 21.0 and 16.1 ppm, with two more intense peaks at 14.9 and 12.9 ppm. The $^2B_{2g}$ state of IsdI−heme−CN exhibits no intense peaks downfield of 12 ppm, whereas the ^2E_g state of rHO−heme−CN has several resonances in this region, including two assigned to heme methyl groups. Thus, the downfield hyperfine-shifted resonances of MhuD−heme−CN suggest that there may be significant population of a ^2E_g state in MhuD−heme−CN at 25 °C. However, the MhuD−heme−CN ^{1}H NMR spectrum also contains several far upfield hyperfine-shifted resonances. These peaks have no counterparts in the spectrum of rHO−heme−CN, but upfield resonances have been assigned to the heme meso protons of IsdI−heme−CN. It is likely that some of the upfield resonances observed in the ^{1}H NMR spectrum of MhuD−heme−CN arise from heme meso protons and that there is significant population of a $^2B_{2g}$ state at 25 °C.

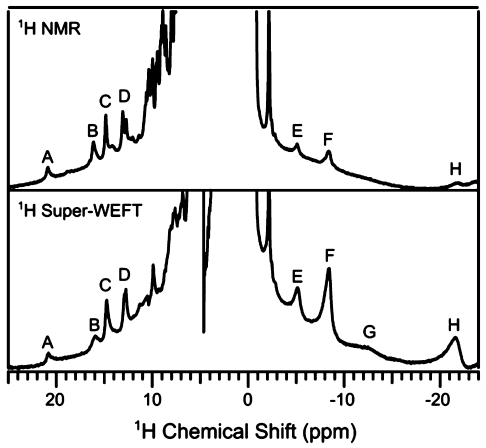

Figure 4. (Top) ^{1}H NMR spectrum of 1.5 mM MhuD−heme−CN in 20 mM NaPi, pH 7.4, (100% D_2O) at 25 °C. (Bottom) ^{1}H Super-WEFT spectrum with a 50 ms τ-delay. The chemical shifts of resonances A−H are reported as a function of temperature in Figure 5.

Our observation of some resonances consistent with a ^2E_g state and others with a $^2B_{2g}$ state in the ^{1}H NMR spectrum of MhuD−heme−CN suggests that more than one $S = {}^1/_2$ state may be populated at room temperature. In this case, because spin-allowed electronic transitions are fast on the NMR time scale, ^{1}H resonances will be observed at the Boltzmann-weighted average of the chemical shifts for the two states. Additionally, the temperature dependence of the observed shifts will deviate from the Curie law because the relative populations of the two states are governed by Boltzmann. We monitored the chemical shifts of several hyperfine-shifted resonances as a function of temperature (Figure S6). The hyperfine shift of each resonance decreases with increasing temperature, as would be expected for a paramagnetic species. However, when the diamagnetic shifts for these resonances were extrapolated according to the Curie law,[46] all but one of the diamagnetic shifts fell outside of the typical 0−10 ppm range (Figure 5). This indicates that the temperature dependence does not follow the Curie law, which is consistent with population of two or more electronic states at room

dx.doi.org/10.1021/ic500033b | Inorg. Chem. 2014, 53, 5931−5940

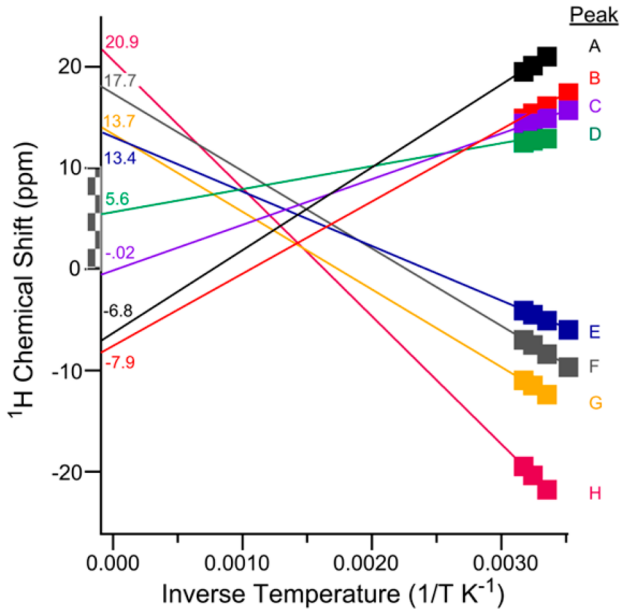

Figure 5. Curie law plot for ^{1}H resonances A–H of MhuD–heme–CN. The squares represent the experimental data at 11, 25, 35, and 42 °C. The lines represent a fit to the Curie law. For seven of the eight resonances, the Curie law extrapolation to infinite temperature predicts a diamagnetic shift outside of the 0–10 ppm region. This indicates that more than one $S = {}^1/_2$ state is populated at room temperature.

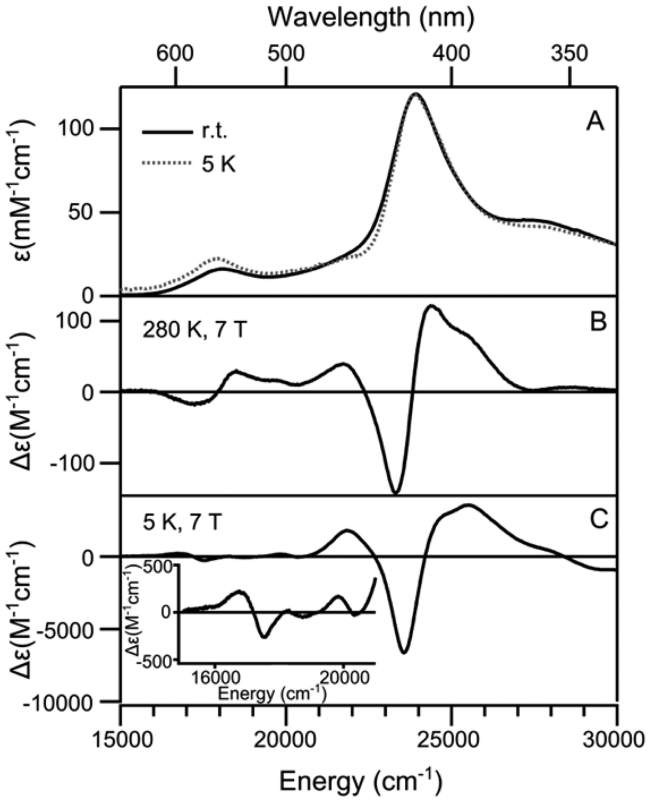

Figure 6. (A) Abs spectra of MhuD–heme–CN in 20 mM Tris, pH 7.4, 50 mM NaCl at room temperature (solid line) and in 50 mM KPi, pH 7.4, 50 mM NaCl, 60% glycerol at 5 K (dotted line). (B) 280 K, 7 T MCD spectrum of MhuD–heme–CN in 40 mM KPi, pH 7.4, 40 mM NaCl, 60% glycerol. (C) 5 K, 7 T MCD spectrum of MhuD–heme–CN in 50 mM KPi, pH 7.4, 50 mM NaCl, 60% glycerol.

temperature. Unfortunately, the broadness of the hyperfine-shifted resonances has prevented acquisition of adequate two-dimensional NMR data for ^{1}H resonance assignments. In this work, we employ VTVH MCD spectroscopy to aid our identification of the MhuD–heme–CN electronic ground state.

Room-Temperature Optical Spectroscopy. Before investigating the electronic structure of MhuD–heme–CN at cryogenic temperatures using optical spectroscopy, we acquired Abs and MCD spectra at room temperature (Figure 6A,B). The Abs spectrum of MhuD–heme–CN is similar to those of both rHO–heme–CN and IsdI–heme–CN, with a Q-band near 18 100 cm^{-1} and a Soret band at 23 900 cm^{-1}.[30,47] Both of these bands are attributed to electronic transitions from occupied porphyrin π-based MOs to unoccupied porphyrin π^*-based MOs.[48] As noted previously,[6] the energy of the MhuD–heme–CN Q-band is more similar to that of IsdI–heme–CN (17 900 cm^{-1}) than that of rHO–heme–CN (18 700 cm^{-1}). The Soret band energy measured for MhuD–heme–CN (23 900 cm^{-1}) is identical to that of rHO–heme–CN and blue-shifted by 100 cm^{-1} from that of IsdI–heme–CN. Overall, the room-temperature Abs data suggests that the electronic structure of MhuD–heme–CN may be more similar to that of IsdI–heme–CN than to that of rHO–heme–CN. However, the differences between the room-temperature Abs spectra of rHO–heme–CN and IsdI–heme–CN are not significant enough to unambiguously determine the electronic ground state of MhuD–heme–CN based on Abs data alone.

The 280 K, 7 T MCD spectrum of MhuD–heme–CN is remarkably similar to the 293 K, 1 T MCD spectrum of IsdI–heme–CN (Figure 6B).[30] The lowest-energy feature in the MCD spectrum of MhuD–heme–CN is the derivative-shaped Q-band, which crosses the zero line at 17 900 cm^{-1}. This is nearly identical in shape and energy to the MCD-detected Q-band of IsdI–heme–CN. In contrast, the Q-band in the 274 K, 1.4 T MCD spectrum of rHO–heme–CN is a negatively signed, absorptive-shaped peak centered at 17 600 cm^{-1}.[47] On the high-energy side of the Q-band, the MCD spectra of both MhuD–heme–CN and IsdI–heme–CN exhibit two positively signed bands near 20 000 and 22 000 cm^{-1}, plus a derivative-shaped Soret band that crosses the zero line at 23 800 cm^{-1}. In the MCD spectrum of rHO–heme–CN, no positively signed bands are apparent between the Q and Soret bands, and the zero crossing point of the Soret band is 24 100 cm^{-1}. On the basis of the room-temperature optical data alone, it would appear that the electronic ground state of MhuD–heme–CN at room temperature is $^2B_{2g}$, similar to IsdI–heme–CN, but this conclusion is inconsistent with the NMR spectroscopic data (Figure 4). To better identify the electronic ground state of MhuD–heme–CN, we utilized Abs and MCD spectroscopy at cryogenic temperatures.

Cryogenic-Temperature Optical Spectroscopy. The room-temperature and 5 K Abs spectra of MhuD–heme–CN are nearly identical (Figure 6A), confirming that we have not significantly perturbed the porphyrin electronic structure by cooling the system to 5 K. However, the 280 K, 7 T and 5 K, 7 T MCD spectra are quite different (Figure 6B,C). The MCD spectrum is an order of magnitude more intense at 5 K, as would be expected for a paramagnetic species with *C*-term contributions to the MCD intensity.[42] In addition, the individual bands are narrower at 5 K, presumably because of decreased vibronic contributions, and, most significantly,

dx.doi.org/10.1021/ic500033b | Inorg. Chem. 2014, 53, 5931–5940

several bands shift to different energies. The lowest-energy bands at 5 K are distinct from those observed at room temperature, with an initial positive peak at 16 800 cm^{-1} followed by negative troughs at 17 500 and 18 700 cm^{-1}. At higher energies, the 5 K MCD spectrum exhibits a positive transition at 19 800 cm^{-1} and a trough at 20 300 cm^{-1}, as opposed to all positive peaks observed in the 280 K spectrum. Finally, upon lowering the temperature from 280 to 5 K, the derivative-shaped Soret band blue-shifts by 400 cm^{-1} from 23 800 to 24 200 cm^{-1}, similar to the energy of the Soret band in the 274 K MCD spectrum of rHO–heme–CN.[47] However, it is important to note that the MCD intensity for a ^2E_g state is an order of magnitude greater than that of a $^2B_{2g}$ state.[43] This is because the components of a ^2E_g state can gain C-term intensity from spin–orbit coupling between the two components of the ^2E_g set, but the $^2B_{2g}$ state has no mixing states of appropriate symmetry. As a result, the fact that transitions originating from a ^2E_g state dominate the MCD spectrum at 5 K simply means that this state is significantly populated at 5 K and the 5 K, 7 T MCD spectral data for MhuD–heme–CN is consistent with either a ^2E_g or a $^2B_{2g}$ electronic ground state.

In order to distinguish between ^2E_g and $^2B_{2g}$ electronic ground states, we measured VTVH MCD saturation curves for the Soret band trough (424 nm) of MhuD–heme–CN at 2, 5, and 10 K (Figure 7). The curves for MhuD–heme–CN closely

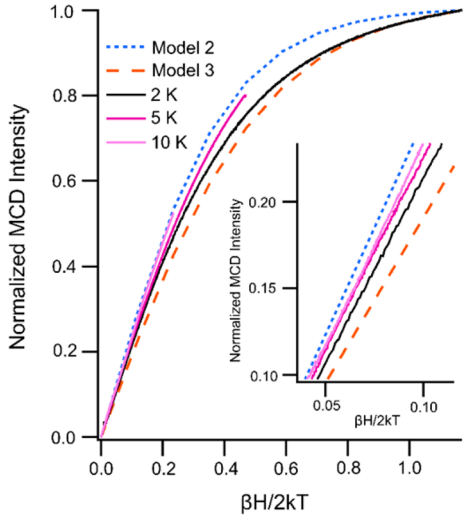

Figure 7. VTVH MCD saturation magnetization curves recorded at 2, 5, and 10 K for MhuD–heme–CN along with simulated saturation magnetization curves for two low-spin Fe(III) model complexes.[43] The VTVH MCD data strongly suggests that the electronic ground state of MhuD–heme–CN is $^2B_{2g}$ and that there exists a low-lying ^2E_g electronic excited state.

align with an $S = {}^1/_2$ iron center.[42] However, there is some nesting of the saturation magnetization curves. Nesting of saturation magnetization curves is typically associated with either a high-spin system or coupled-spin systems. On the basis of the π^* acceptor strength of a cyanide ligand, it is extremely unlikely that an Fe(III)–CN complex would form a high-spin species. Indeed, the MhuD–heme–CN curves do not align with those of a high-spin complex (Figure S7). If the nesting of the MhuD–heme–CN saturation magnetization arises from a coupled spin system, then it would most likely be a small fraction of MhuD–diheme–CN. The MhuD–diheme–CN curves are less nested than the MhuD–heme–CN curves, indicating that a MhuD–diheme–CN fraction is not the source of nesting in the MhuD–heme–CN data (Figure S8). Although nesting is unusual for an isolated $S = {}^1/_2$ center, it is possible if a thermal mixture of two or more $S = {}^1/_2$ states are populated. On the basis of the NMR and MCD spectroscopic data presented up to this point, this is a realistic possibility for MhuD–heme–CN. To investigate this possibility further, we simulated VTVH MCD saturation magnetization curves for two Fe(III) porphyrin model complexes, one with a ^2E_g electronic ground state and the other with a $^2B_{2g}$ ground state.

VTVH MCD saturation magnetization curves for *xy*-polarized transitions of two ferric tetramesitylporphyrin (TMP) complexes were simulated at 2 K based on previously reported g values measured by EPR spectroscopy (Figure 7).[43] Model 2 has a ^2E_g ground state, and model 3 has a $^2B_{2g}$ ground state. The initial slope of the VTVH MCD saturation magnetization curve for the ^2E_g model is steeper than that for the $^2B_{2g}$ model. This is because the initial slope for an *xy*-polarized transition is proportional to the g_z value,[42] which is ~3.0 for the ^2E_g model and ~1.5 for the $^2B_{2g}$ model. The initial slope of the 2 K VTVH MCD saturation magnetization curve for MhuD–heme–CN is intermediate of the ^2E_g and $^2B_{2g}$ curves. As the temperature is raised, the initial slope of the saturation magnetization curve increases, consistent with greater population of a ^2E_g excited state. Thus, a picture emerges whereby MhuD–heme–CN most likely has a $^2B_{2g}$ electronic ground state with a very low-lying ^2E_g excited state.

DISCUSSION

Geometric Structure of MhuD–heme–CN. It has been suggested that the heme ruffling observed in structures of IsdG-like heme-degrading proteins is required for their activity.[30,32] The Cα atoms of the MhuD–heme–CN structure superimpose with those of N7A IsdG (PDB ID 2ZDO) and IsdI–heme–CN (PDB ID 3QGP), with rmsd's of 1.59 and 1.24 Å, respectively (Figure 8, IsdG is not shown for clarity).[30,31] The 1.5 Å distortion of heme from planarity in the MhuD–heme–CN structure is less than that observed for N7A IsdG and IsdI–heme–CN, which show heme distortions of 1.9 and 2.3 Å, respectively (Figure S9). In contrast, the overall out-of-plane distortion (1.5 Å) and the degree of heme ruffling (1.4 Å) in MhuD–heme–CN are more than that observed in rHO–heme–CN (PDB ID 2E7E) at pH 6.8,[44] which displays only 0.6 Å distortion from planarity and 0.5 Å ruffling (Figure S9). Finally, although the bound hemes of MhuD–heme–CN, IsdG, and IsdI occupy similar positions within their respective structures, the entire heme molecule, thus including the propionate groups, for both IsdG and IsdI are rotated approximately 90° about the axis normal to the tetrapyrrole ring compared to the MhuD-bound heme (Figure 8B). The positional difference within the heme molecules is dictated by the α1 helix and the loop region directly following the α2 helix. Within MhuD–heme–CN, the C-terminus of the α1 helix has an additional turn as compared to that of heme-bound IsdG/I, which enables Arg26 to form a H-bonding network with a water molecule, His75, and heme propionates 6 and 7. The last turn of this α1 helix is a loop region in both the IsdG and IsdI structures and thus the IsdG/I Arg26 Cα is displaced ~6 Å from the heme molecule, with its side chain solvent accessible instead of participating within the active site, as observed for Arg26 in the MhuD–heme–CN structure (Figures 3B and 8B). Furthermore, the structural variance in the loop region directly following the α2 helix combined with that of the α1

dx.doi.org/10.1021/ic500033b | Inorg. Chem. 2014, 53, 5931–5940

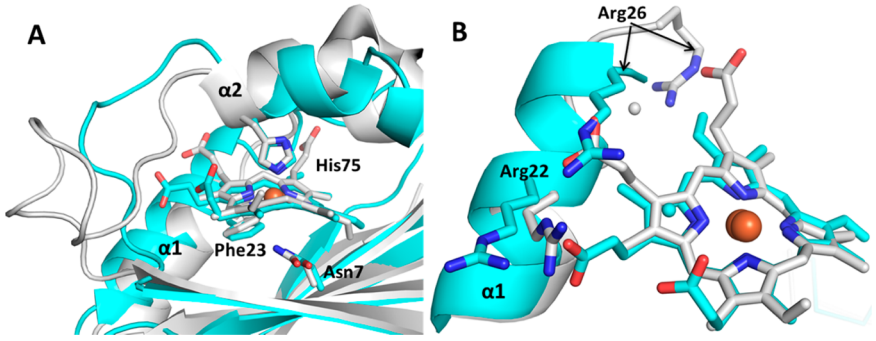

Figure 8. Structural comparison of MhuD−heme−CN with IsdI−heme−CN. (A) Superposition of MhuD−heme−CN (cyan, PDB ID 4NL5) with IsdI−heme−CN (white, PDB ID 3QGP) shows that the orientation of heme within the active site of MhuD is different compared to that of IsdG and IsdI, whereby the heme propionates in MhuD are rotated 90° around the axis normal to the heme plane. (B) The final turn of the α1 helix of MhuD (contains Arg26) is a loop region in the IsdI structure, enabling IsdI Arg26 to flip from within the active site, as observed in MhuD, to be surface-exposed. Residue side chains and heme molecules are represented as sticks, with oxygen, nitrogen, and iron atoms colored red, blue, and orange, respectively. Ordered water molecules are represented as spheres.

helix results in the MhuD heme propionates pointing toward this loop region, whereas the corresponding propionates in IsdG/I point toward the α1 helix, reducing their solvent accessibility compared to those of MhuD (Figure 8). This heme rotation may play a role in the variant location of tetrapyrrole ring cleavage during the heme degradation reaction of MhuD and IsdG/I proteins, whereby the two products of IsdG/I indicate cleavage at the β- and δ-meso carbons and the products of MhuD indicate cleavage at the α-meso carbon.[6,19] The kink observed in the α2 helix of MhuD−heme−CN is reminiscent of the corresponding helix in the *S. aureus* IsdG and IsdI heme-degrading proteins.[31]

Electronic Structure of MhuD−heme−CN. Whereas the electronic structures of HO−heme−CN and IsdI−heme−CN are dominated by single electronic states at physiologically relevant temperatures,[18,25,26,30] at least two $S = {}^1/_2$ electronic states are significantly populated in MhuD−heme−CN. The electronic ground state of MhuD−heme−CN is $^2B_{2g}$, similar to that of IsdI−heme−CN, and the populated excited state is ^2E_g, similar to the ground state of HO−heme−CN. In both electronic states, five electrons are distributed among the Fe $3d_{xy}$-, $3d_{xz}$-, and $3d_{yz}$-based MOs, and the relative energies of these MOs determine the state populations at room temperature. In HO−heme−CN, the Fe $3d_{xy}$-based MO is lower in energy than the Fe $3d_{xz}$- and $3d_{yz}$-based MOs; the unpaired electron is placed in either $3d_{xz}$ or $3d_{yz}$ and delocalized onto the porphyrin pyrrole rings (Figure 1).[49] The opposite case is observed for IsdI−heme−CN. The Fe $3d_{xy}$-based MO is higher in energy, singly occupied, and the spin density is delocalized onto the porphyrin meso carbons.[50] In MhuD−heme−CN, there is exchange between the two electronic states, and spin density is delocalized onto either the porphyrin pyrrole rings or the porphyrin meso carbons depending upon the electronic configuration at a given point in time.

The varying degrees of heme ruffling in the X-ray crystal structures of MhuD−heme−CN (PDB ID 4NL5), rHO−heme−CN (PDB ID 2E7E),[44] and IsdI−heme−CN (PDB ID 3QGP)[30] provide insight into the differences between their electronic structures (Figure S9). The Fe $3d_{xy}$-, $3d_{xz}$-, and $3d_{yz}$-based MOs are all energetically destabilized by porphyrin ruffling,[51] but the greatest destabilization is experienced by the Fe $3d_{xy}$-based MO. Ruffling increases the overlap between the Fe $3d_{xy}$ orbital and the porphyrin a_{2u} orbital. This lowers the energy of the bonding combination, the occupied porphyrin a_{2u}-based MO, and raises the energy of the anti-bonding combination, the Fe $3d_{xy}$-based MO. When the magnitude of heme ruffling is increased from 0.5 Å in rHO−heme−CN to 2.3 Å in IsdI−heme−CN, the Fe $3d_{xy}$-based MO moves to a higher energy than the Fe $3d_{xz}$- and $3d_{yz}$-based MOs, and the electronic ground state changes from ^2E_g to $^2B_{2g}$ (Figure 9). When the degree of heme ruffling is only increased to 1.4 Å, as is the case for MhuD−heme−CN, the energy of the Fe $3d_{xy}$-based MO is only slightly greater than those of the Fe $3d_{xz}$- and $3d_{yz}$-based MOs, and both electronic states are significantly populated at room temperature. For the His−heme−CN moiety, the crossover point where heme ruffling changes the ground state from ^2E_g to $^2B_{2g}$ must be somewhere between 0.5 and 1.4 Å of ruffling.

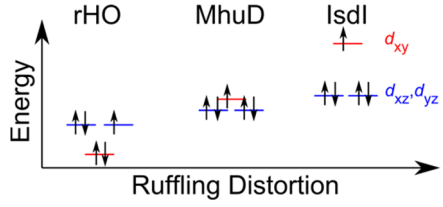

Figure 9. Porphyrin ruffling alters the relative energies of the Fe $3d_{xy}$-, $3d_{xz}$-, and $3d_{yz}$-based MOs. As the degree of ruffling increases from 0.5 Å (rHO−heme−CN) to 2.3 Å (IsdI−heme−CN), the electronic ground state changes from ^2E_g to $^2B_{2g}$. MhuD−heme−CN exhibits an intermediate degree of ruffling (1.4 Å), and consequently a thermal mixture of these two states is observed.

Implications for MhuD-Catalyzed Heme Degradation. In *S. aureus* IsdI, it has been concluded that heme ruffling contributes to heme-degradation activity,[32] but it remains unclear if the relationship between ruffling and activity is due to structural and/or electronic considerations. The X-ray crystal structure of MhuD−heme−CN provides insight into the structural contributions to the regioselectivity of MhuD-catalyzed heme degradation. Porphyrin ruffling displaces all four heme meso carbons out of the heme plane. This distortion places α- and γ-meso carbons on the distal side of the heme plane, whereas the β- and δ-meso carbons are pushed away from the distal ligand and toward the proximal His ligand. As suggested previously based on examination of the MhuD−diheme X-ray crystal structure (PDB ID 3HX9);[5,6] this pattern of meso carbon distortion is opposite that observed in IsdG/I

dx.doi.org/10.1021/ic500033b | *Inorg. Chem.* 2014, 53, 5931−5940

because of 90° in-plane rotation of the heme substrate relative to its orientation in IsdG/I. The proximities of the α- and γ-meso carbons to the distal ligand site make these meso carbons significantly more accessible to reactive iron−dioxygen species in MhuD, whereas the β- and δ-meso carbons are more accessible to reactive iron−dioxygen species in IsdG/I. This distortion would seem to suggest that α-meso carbon oxygenation by MhuD occurs prior to β- or δ-meso carbon oxygenation.

It is likely that there is also a significant electronic contribution to the regioselectivity of heme cleavage by MhuD, as structural considerations do not explain the selectivity for the for the α-meso carbon over the γ-meso carbon. In *S. aureus* IsdI, heme cleavage can occur at both meso carbons pushed out of the plane toward the distal ligand site,[19,20] but in *M. tuberculosis*, MhuD ring cleavage occurs only at the α-meso carbon.[6] One contribution to the α-regioselectivity of porphyrin cleavage by most canonical HOs is steric protection of the β-, δ-, and γ-meso carbons by the distal helix, as first noted in the X-ray crystal structure of human HO (PDB ID 1N45),[9] and a similar steric origin for α-regioselctivity was proposed for the reaction catalyzed by MhuD prior to the solution of the MhuD−heme−CN X-ray crystal structure.[6] However, the distal faces of both the α- and γ-meso carbons have similar degrees of hydrophobic protection by Val53 in the case of the α-meso carbon and Ile9 in the case of the γ-meso carbon. It is also unlikely that the distal ligand tilt is a significant contributor to regioselectivity. In the MhuD−heme−CN X-ray crystal structure, the terminal nitrogen of the CN ligand is only 0.08 Å closer to the γ-meso carbon than to the α-meso carbon. In the absence of a satisfying structural explanation, the potential electronic contributions to the reaction catalyzed by MhuD warrant further consideration.

The α-regioselectivity of MhuD-catalyzed heme cleavage can best be explained for a reaction that proceeds through a $^2B_{2g}$ electronic state, similar to the mechanism proposed for IsdI-catalyzed heme degradation.[30,32] In a $^2B_{2g}$ state, spin density is delocalized onto the porphyrin meso carbons because of overlap of the Fe $3d_{xy}$ and C $2p_z$ orbitals.[21] The α-meso carbon is displaced 0.7 Å out of the heme plane normal to the Fe−His bond in the MhuD−heme−CN structure (PDB ID 4NL5), as compared to a 0.4 Å displacement of the γ-meso carbon. As a result, there should be significantly more orbital overlap between the Fe $3d_{xy}$ and α-meso C $2p_z$ orbitals, placing more spin density on the α-meso carbon. This would give the α-meso carbon more partial radical character than the γ-meso carbon and favor selective attack of the α-meso carbon by a reactive iron−dioxygen species.

The possible functional role of the unexpected finding that two $S = {}^1/_2$ states are significantly populated in MhuD−heme−CN at physiologically relevant temperatures warrants consideration. A thermal mixture of $S = {}^3/_2$ and ${}^1/_2$ ferric heme electronic states has been observed previously for hydroxide and azide complexes of *P. aeruginosa* PigA,[52,53] but to our knowledge, this is the first report of a thermal mixture of two $S = {}^1/_2$ ferric heme states in a heme-degrading enzyme. On the basis of the data presented in this work and in the literature,[30,32] it appears that the first porphyrin oxygenation step in both the MhuD- and IsdI-catalyzed reactions proceeds through a $^2B_{2g}$ electronic state. However, porphyrin oxygenation of a ruffled heme substrate by a reactive iron−dioxygen species generated in the distal pocket of MhuD cannot explain the additional β- or δ-meso oxygenation deduced from the structure of mycobilin.[6] We propose that the structural and electronic plasticity of the MhuD substrate allows the enzyme to pursue a reactive pathway distinct from that of either canonical HOs or IsdG-like heme-degrading enzymes.

■ ASSOCIATED CONTENT

Supporting Information

SDS-PAGE gel for the modified apo-MhuD purification; heme/ascorbate degradation assay for MhuD−heme in 20 mM NaPi, pH 7.8; heme/acsorbate degradation assay for heme without MhuD in 20 mM Tris, pH 7.4, 50 mM NaCl; heme/ascorbate degradation assay for MhuD−heme−CN in 20 mM NaPi, pH 7.4; composite omit electron density map for bound heme−CN; ^{1}H Super-WEFT spectra of 1.5 mM MhuD−heme−CN in 20 mM NaPi, pH 7.4; VTVH MCD saturation magnetization curves of MhuD−heme−CN and high-spin chloro(*meso*-tetraphenylporphinato)iron(III); VTVH MCD saturation magnetization curves for MhuD−heme−CN and MhuD−diheme−CN; degree of heme ruffling within heme degrading enzymes; and crystallographic data in CIF format. This material is available free of charge via the Internet at http://pubs.acs.org.

■ AUTHOR INFORMATION

Corresponding Author

*E-mail: matthew.liptak@uvm.edu. Phone: (802) 656-0161. Fax: (802) 656-8705.

Author Contributions

The manuscript was written through contributions of all authors. All authors have given approval to the final version of the manuscript.

Notes

The authors declare no competing financial interest.

■ ACKNOWLEDGMENTS

M.D.L. thanks the University of Vermont for financial support, C.W.G. thanks the National Institutes of Health for financial support (AI081161), and A.C. thanks the National Science Foundation for predoctoral fellowship support (DGE-1321846). We would like to thank the Advanced Light Source at Berkeley National Laboratories and Stanford Synchrotron Radiation Lightsource (SSRL) and their respective staff for their invaluable help in data collection. A.G. and M.L. would like to thank Prof. Mark Riley (University of Queensland) for providing a free copy of the VTVH MCD simulation program.

■ REFERENCES

(1) Tullius, M. V.; Harmston, C. A.; Owens, C. P.; Chim, N.; Morse, R. P.; McMath, L. M.; Iniguez, A.; Kimmey, J. M.; Sawaya, M. R.; Whitelegge, J. P.; Horwitz, M. A.; Goulding, C. W. *Proc. Natl. Acad. Sci. U.S.A.* **2011**, *108*, 5051−5056.

(2) Jones, C. M.; Niederweis, M. *J. Bacteriol.* **2011**, *193*, 1767−1770.

(3) Owens, C. P.; Du, J.; Dawson, J. H.; Goulding, C. W. *Biochemistry* **2012**, *51*, 1518−1531.

(4) Owens, C. P.; Chim, N.; Graves, A. B.; Harmston, C. A.; Iniguez, A.; Contreras, H.; Liptak, M. D.; Goulding, C. W. *J. Biol. Chem.* **2013**, *288*, 21714−21728.

(5) Chim, N.; Iniguez, A.; Nguyen, T. Q.; Goulding, C. W. *J. Mol. Biol.* **2010**, *395*, 595−608.

(6) Nambu, S.; Matsui, T.; Goulding, C. W.; Takahashi, S.; Ikeda-Saito, M. *J. Biol. Chem.* **2013**, *288*, 10101−10109.

(7) Tullius, M. V.; Harth, G.; Maslesa-Galic, S.; Dillon, B. J.; Horwitz, M. A. *Infect. Immun.* **2008**, *76*, 5200−5214.

(8) Owens, C. P.; Chim, N.; Goulding, C. W. *Future Med. Chem.* **2013**, *5*, 1391−1403.

(9) Schuller, D. J.; Wilks, A.; Ortiz de Montellano, P. R.; Poulos, T. L. *Nat. Struct. Biol.* **1999**, *6*, 860−867.
(10) Sugishima, M.; Omata, Y.; Kakuta, Y.; Sakamoto, H.; Noguchi, M.; Fukuyama, K. *FEBS Lett.* **2000**, *471*, 61−66.
(11) Bianchetti, C. M.; Yi, L.; Ragsdale, S. W.; Phillips, G. N. *J. Biol. Chem.* **2007**, *282*, 37624−37631.
(12) Schuller, D. J.; Zhu, W.; Stojiljkovic, I.; Wilks, A.; Poulos, T. L. *Biochemistry* **2001**, *40*, 11552−11558.
(13) Hirotsu, S.; Chu, G. C.; Unno, M.; Lee, D.-S.; Yoshida, T.; Park, S.-Y.; Shiro, Y.; Ikeda-Saito, M. *J. Biol. Chem.* **2004**, *279*, 11937−11947.
(14) Friedman, J.; Lad, L.; Li, H.; Wilks, A.; Poulos, T. L. *Biochemistry* **2004**, *43*, 5239−5245.
(15) Wu, R.; Skaar, E. P.; Zhang, R.; Joachmiak, G.; Gornicki, P.; Schneewind, O.; Joachmiak, A. *J. Biol. Chem.* **2005**, *280*, 2840−2846.
(16) Wilks, A.; Heinzl, G. *Arch. Biochem. Biophys.* **2014**, *544*, 87−95.
(17) Ratliff, M.; Zhu, W.; Deshmukh, R.; Wilks, A.; Stojiljkovic, I. *J. Bacteriol.* **2001**, *183*, 6394−6403.
(18) Caignan, G. A.; Deshmukh, R.; Wilks, A.; Zeng, Y.; Huang, H.; Moënne-Loccoz, P.; Bunce, R. A.; Eastman, M. A.; Rivera, M. *J. Am. Chem. Soc.* **2002**, *124*, 14879−14892.
(19) Reniere, M. L.; Ukpabi, G.; Harry, S. R.; Stec, D. F.; Krull, R.; Wright, D. W.; Bachmann, B. O.; Murphy, M. E. P.; Skaar, E. P. *Mol. Microbiol.* **2010**, *75*, 1529−1538.
(20) Matsui, T.; Nambu, S.; Ono, Y.; Goulding, C. W.; Tsumoto, K.; Ikeda-Saito, M. *Biochemistry* **2013**, *52*, 3025−3027.
(21) Rivera, M.; Caignan, G. A.; Astashkin, A. V.; Raitsimring, A. M.; Shokhireva, T. K.; Walker, F. A. *J. Am. Chem. Soc.* **2002**, *124*, 6077−6089.
(22) Garcia-Serres, R.; Davydov, R. M.; Matsui, T.; Ikeda-Saito, M.; Hoffman, B. M.; Huynh, B. H. *J. Am. Chem. Soc.* **2007**, *129*, 1402−1417.
(23) Chen, H.; Moreau, Y.; Derat, E.; Shaik, S. *J. Am. Chem. Soc.* **2008**, *130*, 1953−1965.
(24) For convenience and historical consistency, we will label all molecular orbitals and electronic states according to their representations in the D_{4h} point group. However, it is important to note that the Fe-porphyrin chromophore has only approximate D_{4h} symmetry.
(25) Gorst, C. M.; Wilks, A.; Yeh, D. C.; Ortiz de Montellano, P. R.; La Mar, G. N. *J. Am. Chem. Soc.* **1998**, *120*, 8875−8884.
(26) Ogura, H.; Evans, J. P.; Peng, D.; Satterlee, J. D.; Ortiz de Montellano, P. R.; La Mar, G. N. *Biochemistry* **2009**, *48*, 3127−3137.
(27) Li, Y.; Syvitski, R. T.; Auclair, K.; Wilks, A.; Ortiz de Montellano, P. R.; La Mar, G. N. *J. Biol. Chem.* **2002**, *277*, 33018−33031.
(28) Syvitski, R. T.; Li, Y.; Auclair, K.; Ortiz de Montellano, P. R.; La Mar, G. N. *J. Am. Chem. Soc.* **2002**, *124*, 14296−14297.
(29) Li, Y.; Syvitski, R. T.; Auclair, K.; Ortiz de Montellano, P. R.; La Mar, G. N. *J. Am. Chem. Soc.* **2003**, *125*, 13392−13403.
(30) Takayama, S. J.; Ukpabi, G.; Murphy, M. E.; Mauk, A. G. *Proc. Natl. Acad. Sci. U.S.A.* **2011**, *108*, 13071−13076.
(31) Lee, W. C.; Reniere, M. L.; Skaar, E. P.; Murphy, M. E. *J. Biol. Chem.* **2008**, *283*, 30957−30963.
(32) Ukpabi, G.; Takayama, S. J.; Mauk, A. G.; Murphy, M. E. *J. Biol. Chem.* **2012**, *287*, 34179−34188.
(33) Dawson, R. M.; Elliot, C. D.; Elliot, W. H.; Jones, M. K. *Data for Biochemical Research*; Clarendon Press: Oxford, UK, 1986; pp 230−231.
(34) Berry, E. A.; Trumpower, B. L. *Anal. Biochem.* **1987**, *161*, 1−15.
(35) Battye, T. G. G.; Kontogiannis, L.; Johnson, O.; Powell, H. R.; Leslie, A. G. W. *Acta Crystallogr., Sect. D: Biol. Crystallogr.* **2011**, *67*, 271−281.
(36) Adams, P. D.; Afonine, P. V.; Bunkóczi, G.; Chen, V. B.; Davis, I. W.; Echols, N.; Headd, J. J.; Hung, L.-W.; Kapral, G. J.; Grosse-Kunstleve, R. W.; McCoy, A. J.; Moriarty, N. W.; Oeffner, R.; Read, R. J.; Richardson, D. C.; Richardson, J. S.; Terwilliger, T. C.; Zwart, P. H. *Acta Crystallogr., Sect. D: Biol. Crystallogr.* **2010**, *66*, 213−221.
(37) Emsley, P.; Lohkamp, B.; Scott, W. G.; Cowtan, K. *Acta Crystallogr., Sect. D: Biol. Crystallogr.* **2010**, *66*, 486−501.
(38) *The PyMOL Molecular Graphics System*, version 1.0; Schrödinger, LLC.
(39) Patt, S. L.; Sykes, B. D. *J. Chem. Phys.* **1972**, *56*, 3182−3184.
(40) Inubushi, T.; Becker, E. D. *J. Magn. Reson.* **1983**, *51*, 128−133.
(41) Riley, M. J. *VTVH − A program for simulation and fitting variable temperature−variable field MCD spectra*; http://vtvh.sourceforge.net/.
(42) Neese, F.; Solomon, E. I. *Inorg. Chem.* **1999**, *38*, 1847−1865.
(43) Cheesman, M. R.; Walker, F. A. *J. Am. Chem. Soc.* **1996**, *118*, 7373−7380.
(44) Sugishima, M.; Oda, K.; Ogura, T.; Sakamoto, H.; Noguchi, M.; Fukuyama, K. *Acta Crystallogr., Sect. F: Struct. Biol. Cryst. Commun.* **2007**, *63*, 471−474.
(45) Jentzen, W.; Song, X.-Z.; Shelnutt, J. A. *J. Phys. Chem. B* **1997**, *101*, 1684−1699.
(46) Shokhirev, N. V.; Walker, F. A. *J. Phys. Chem.* **1995**, *99*, 17795−17804.
(47) Hawkins, B. K.; Wilks, A.; Powers, L. S.; Ortiz de Montellano, P. R.; Dawson, J. H. *Biochim. Biophys. Acta, Protein Struct. Mol. Enzymol.* **1996**, *1295*, 165−173.
(48) Gouterman, M. *J. Chem. Phys.* **1959**, *30*, 1139−1161.
(49) Shokhirev, N. V.; Walker, F. A. *J. Biol. Inorg. Chem.* **1998**, *3*, 581−594.
(50) Nakamura, M. *Coord. Chem. Rev.* **2006**, *250*, 2271−2294.
(51) Liptak, M. D.; Wen, X.; Bren, K. L. *J. Am. Chem. Soc.* **2010**, *132*, 9753−9763.
(52) Caignan, G. A.; Deshmukh, R.; Zeng, Y.; Wilks, A.; Bunce, R. A.; Rivera, M. *J. Am. Chem. Soc.* **2003**, *125*, 11842−11852.
(53) Zeng, Y.; Caignan, G. A.; Bunce, R. A.; Rodriguez, J. C.; Wilks, A.; Rivera, M. *J. Am. Chem. Soc.* **2005**, *127*, 9794−9807.